

The Water Maser in MG 0414+0534: The Influence of Gravitational Microlensing

H. Garsden^{1*}, G. F. Lewis^{1*} and L. Harvey-Smith^{1,2*†}

¹*Sydney Institute for Astronomy, School of Physics, A28, The University of Sydney, NSW 2006, Australia*

²*CSIRO Astronomy and Space Science, Australia Telescope National Facility, PO Box 76, Epping, NSW, 2121, Australia*

Accepted 2010 December 17

ABSTRACT

Water masers have been observed in several high redshift active galactic nuclei, including the gravitationally lensed quasar MG 0414+0534. This quasar is lensed into four images, and the water maser is detected in two of them. The broadening of the maser emission line and its velocity offset are consistent with a group of masers associated with a quasar jet. If the maser group is microlensed we can probe its structure and size by observing its microlensing behaviour over time. We present results of a high resolution numerical analysis of microlensing of the maser in MG 0414+0534, using several physically motivated maser models covering a range of sizes and emission profiles. Time-varying spectra of the microlensed maser are generated, displayed, and analysed, and the behaviour of the different models compared. The observed maser line in MG 0414+0534 is consistent with maser spots as in other quasar jets, provided substructure is de-magnified or currently lost in noise; otherwise smooth extended maser models are also candidates to generate the observed spectrum. Using measures of spectral variability we find that if the maser has small substructure of ~ 0.002 pc then a variation of 0.12 mag in flux and 2.0 km s^{-1} in velocity centroid of the maser line could be observed within 2 decades. For the smallest maser model in this study a magnification of > 35 is possible 22% of the time, which is of significance in the search for other lensed masers.

Key words: quasars: individual: MG 0414+0534 – gravitational lensing – masers – methods: numerical – methods: statistical

1 INTRODUCTION

Gravitational lensing occurs when light travelling to Earth from distant sources is deflected by the gravitational influence of an intervening massive object (Schneider, Ehlers & Falco 1992; Wambsganss 1998). The light source may be within the Galaxy and lensed by planetary systems, which is useful in the search for planets (e.g. Gaudi et al. 2008); or it may be from a very distant galaxy and lensed by another galaxy (e.g. Willis et al. 2006) or galaxy cluster (e.g. Sand, Treu, Elliss et al. 2008). In this paper we are concerned with a quasar being lensed by a galaxy, many instances of which have been discovered (e.g. Walsh, Carswell & Weymann 1979; Huchra et al. 1985; Turner et al. 1989; Myers et al. 1999; Inada et al. 2005;

Kayo, Inada, Oguri et al. 2010). In such systems, multiple magnified images of the quasar are produced, with the image properties determined by the source emission profile, the lensing galaxy’s mass distribution, and the relative position of the source and lens. Assuming a smooth mass distribution for the lensing galaxy is sometimes enough to model the observed image configurations, but in other cases the effect of the compact objects within the galaxy (stars, planets, etc.) must also be considered. Due to the intricate nature of the light paths through a galaxy of myriad objects, a slight change in the location of the background source can produce a change in the image magnifications (independent of any intrinsic source variability). This effect of the compact structure is called *microlensing* (Chang & Refsdal 1979; Young 1981; Paczynski 1986; Wambsganss 1990, 2006a), and identifiable microlensing fluctuations of high amplitude are called *high magnification events*. These events can last for relatively short durations – months or even weeks (Shalyapin 2001) – and usually occur with a frequency of decades.

The angular size of the source is important for microlensing, as larger sources will “wash out” the location-

* E-mail: hgar7294@uni.sydney.edu.au (HG); geraint.lewis@sydney.edu.au (GFL); lisa.harvey-smith@csiro.au (LHS)

† Research undertaken as part of the Commonwealth Cosmology Initiative (CCI: www.thecci.org), an international collaboration supported by the Australian Research Council.

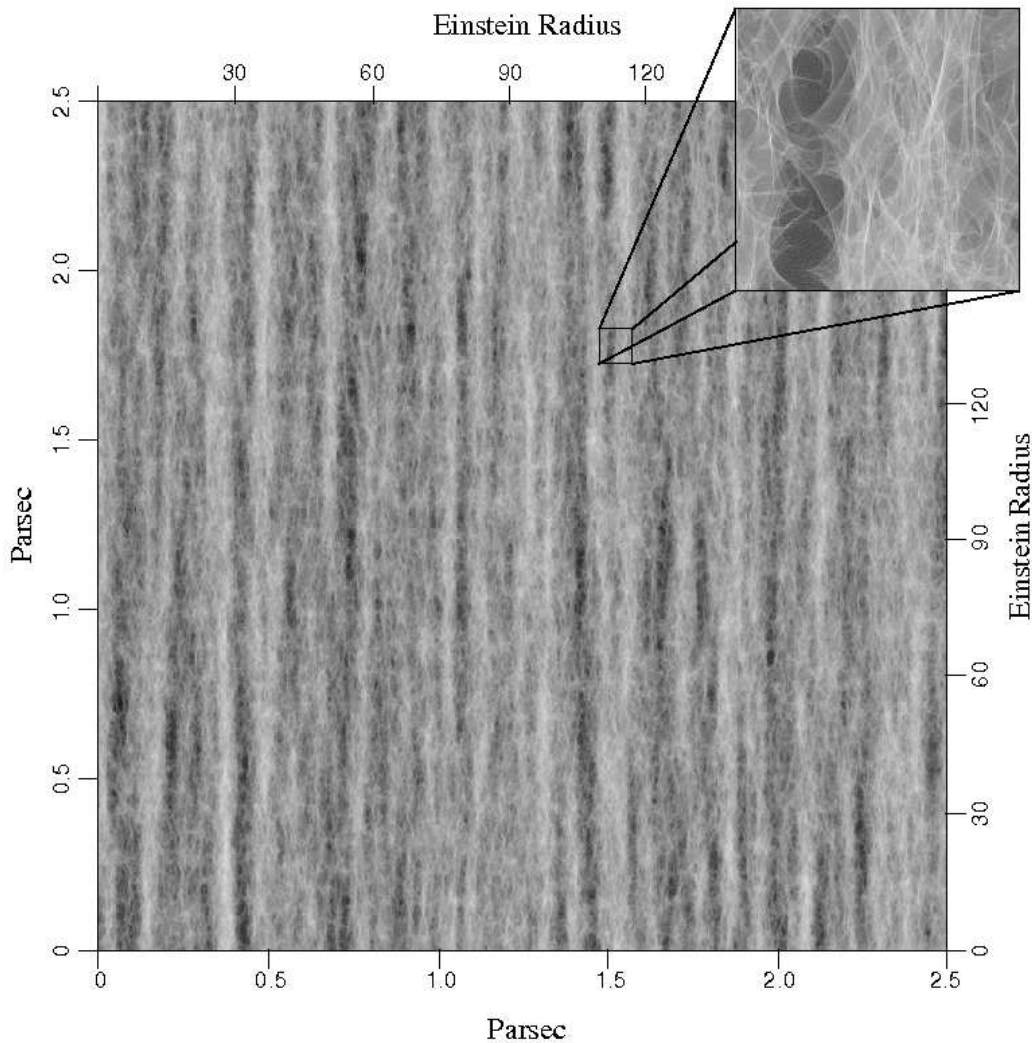


Figure 1. The magnification map representing microlensing variability in image A1, one of the four images of the quasar produced by lensing in MG 0414+0534. The map covers a region of the source plane; at all locations the brightness indicates how much a pixel-sized source would be (de)magnified if the source were at that location. Bright areas indicate high magnification. There are $6,902,710 M_{\odot}$ compact objects in the lens. The map size is $2.5 \times 2.5 \text{ pc}^2$ ($185 \times 185 \text{ ER}^2$) with a resolution of 26 AU. The break-out box is $0.1 \times 0.1 \text{ pc}^2$ ($7.4 \times 7.4 \text{ ER}^2$) at the same resolution. The break-out box shows the high density of caustics in the source plane of this system, and that there are patches where there are no caustics and patches where there are many; these appear as light and dark regions on the larger map. The microlensing parameters used to generate the map are σ (convergence) = 0.472, and γ (shear) = 0.478 (see Section 2.2).

Table 1. Properties of the magnification maps used.

Image	κ	γ	Sidlength	Resolution	Number of lens objects (M_{\odot})
A1	0.472	0.478	2.5 pc (185 ER)	26 AU	3,204,158
			15 pc (1115 ER)	155 AU	115,353,274
A2	0.485	0.550	2.5 pc (185 ER)	26 AU	6,710,081
			15 pc (1115 ER)	155 AU	241,562,900

Four magnification maps were used in this study. Images A1 and A2 were modelled, but there are two maps of different resolutions for each image because there are a range of sizes for the source models. κ (convergence) and γ (shear) are mass parameters from lens models for this system, κ specifies the effect of mass along a light path, and γ specifies the effects of surrounding mass.

induced variability in magnification (Lewis & Gil-Merino 2006; Bate, Webster & Wyithe 2008a), so it is small sources that produce the most significant high magnification events. The shape of the source emission profile also affects microlensing (Mortonson, Schechter, & Wambsganss 2005). Therefore, observations and modelling of flux variability can provide an estimate of source size and flux emission profile. Apparent chromatic effects are also seen (Lewis et al. 1998; Eigenbrod et al. 2008) because if an extended source emits different frequencies from separate regions, the frequencies will be magnified differently, and the source spectrum will be altered. Like the magnification, the spectrum may also change over time, and studying spectral variability can lead to possible spectral emission profiles. In these (and other) ways microlensing becomes a useful tool for astronomical research (Kayser, Refsdal & Stabell 1986; Wambsganss 2006b; Kochanek et al. 2009; Wambsganss 2010).

In this paper we present results of numerical analyses of the microlensing of a water maser in a known microlensing system, MG 0414+0534. We use several physically-motivated models to represent the maser source; each model is characterised by its shape, size, emission and velocity profile. A model is then subjected to numerical microlensing so that the alteration in the spectrum and flux after lensing can be found. The structure of the paper is as follows: Section 2 discusses the maser in MG 0414+0534, and mechanisms used for numerical microlensing analysis. In Section 3 we describe the parameters characterizing the MG 0414+0534 lens, we specify the maser source models, and explain how the models are used. Section 4 presents the results of microlensing of the maser by examining which models induce the most variability, what time scales may be expected for this, what forms the spectra take and how they vary over time, and whether the models match the current observation.

2 BACKGROUND

2.1 The lens and water maser MG 0414+0534

MG 0414+0534 (Lawrence, Elston, Januzzi et al. 1995) is a gravitational lens displaying microlensing (Witt et al. 1995). It consists of a quasar at $z = 2.639$ being lensed by a galaxy at $z = 0.9584$. Recent searches for water masers in six lensed quasars discovered a maser in MG 0414+0534 (Impellizzeri, McKean, Castangia et al. 2008; McKean et al. 2010), indicating the most distant water found in the universe. The emission comes from the $6_{16}-5_{23}$ transition of H_2O at a rest frequency of 22.235 GHz. The observations show a line with a single peak, Doppler broadened by about $\sim 100 \text{ km s}^{-1}$, indicating a spatially extended maser source, offset from the systemic velocity of the quasar by about -300 km s^{-1} . There are four images of the quasar produced in the MG 0414+0534 system, designated A1, A2, B and C, and the maser is observed in A1 and A2. The sensitivity of the telescope was not enough to detect the maser emission in images B and C, which are known to be fainter than A1 and A2.

Most known galactic masers are believed to fall into two categories: disk or jet masers, both of which may be found in the same galaxy and usually consist of groups of “spots”.

Disk masers are generated in a rotating molecular disk around the central engine of an active galaxy and produce a characteristic three-peaked spectrum with blue- and red-shifted components. The canonical example of this configuration is NGC 4258 (Moran, Humphreys, Greenhill et al. 2007). Jet masers are probably generated in turbulent shock fronts around the edges, or at the ends, of AGN radio jets. Such a group of masers will be located some way along the jet and be wholly red- or blue-shifted depending on the jet direction. The masers are typically offset from the AGN core by $\sim 100 \text{ km s}^{-1}$, and have a radial-velocity gradient of $\sim 100 \text{ km s}^{-1} \text{ mas}^{-1}$ in a single direction across the group. The velocity of the masers is not likely to be strongly correlated with the jet velocity for a couple of reasons. Firstly, the jet speed is likely to be a significant fraction of the speed of light (Ros & Kadler 2008), and masers could not survive in such an environment; secondly, the direction of the masers may be influenced by turbulent motion near the jet. Examples of galaxies with jet masers are NGC 1052 (Claussen, Diamond, Braatz et al. 1998) and Mrk 348 (Peck, Henkel, Ulvestad et al. 2003). Based on these two categories, the maser in MG 0414+0534 is most likely to be a jet maser group, since there is only one peak, blue-shifted from the core by 300 km s^{-1} , and a velocity spread of $\sim 100 \text{ km s}^{-1}$. It could be in a jet that is inclined towards us, which is consistent with MG 0414+0534 being a type-1 quasar (Lawrence, Elston, Januzzi et al. 1995).

2.2 Analysis of microlensed quasars

We will adopt a method that has been used previously to study microlensing in MG 0414+0534 and other lensed quasars (e.g. Wambsganss, Paczynski & Schneider 1990; Schechter & Wambsganss 2002; Schechter, Wambsganss & Lewis 2004; Lewis & Gil-Merino 2006; Bate, Floyd, Webster et al. 2008b). Firstly we calculate the microlensing of a point-like source (i.e. the smallest numerically possible) situated in the *source plane* behind the lensing galaxy. The mass distribution in the lens, producing each image, is specified by a convergence (κ) and a shear (γ). The convergence describes the effect of mass near a light ray, and the shear incorporates long-range influences of the overall mass distribution. Values for these parameters for many quasars, including MG 0414+0534, have been determined previously (Witt et al. 1995; Schechter & Wambsganss 2002). Based on these, point masses are laid down randomly over another grid that is the *lens plane*. *Ray-tracing* is then used to find the path of the light as it travels from the source, is deflected through the lens, and reaches the observer. In practice, however, it is more computationally efficient to use light rays that are fired back from the observer through the lens to the source plane. This *inverse ray-tracing* method simultaneously calculates the magnification of the point source for many locations over the source plane.

The result of inverse ray-tracing is a *magnification map* of the source plane, as shown in Figure 1. One map is needed for each image. A map does not encode an image of the quasar that would be seen by us. Rather, each point on the map represents the magnification of a pixel-sized source placed at that location, for all locations over the source plane region being modelled. Brighter areas are high magnification

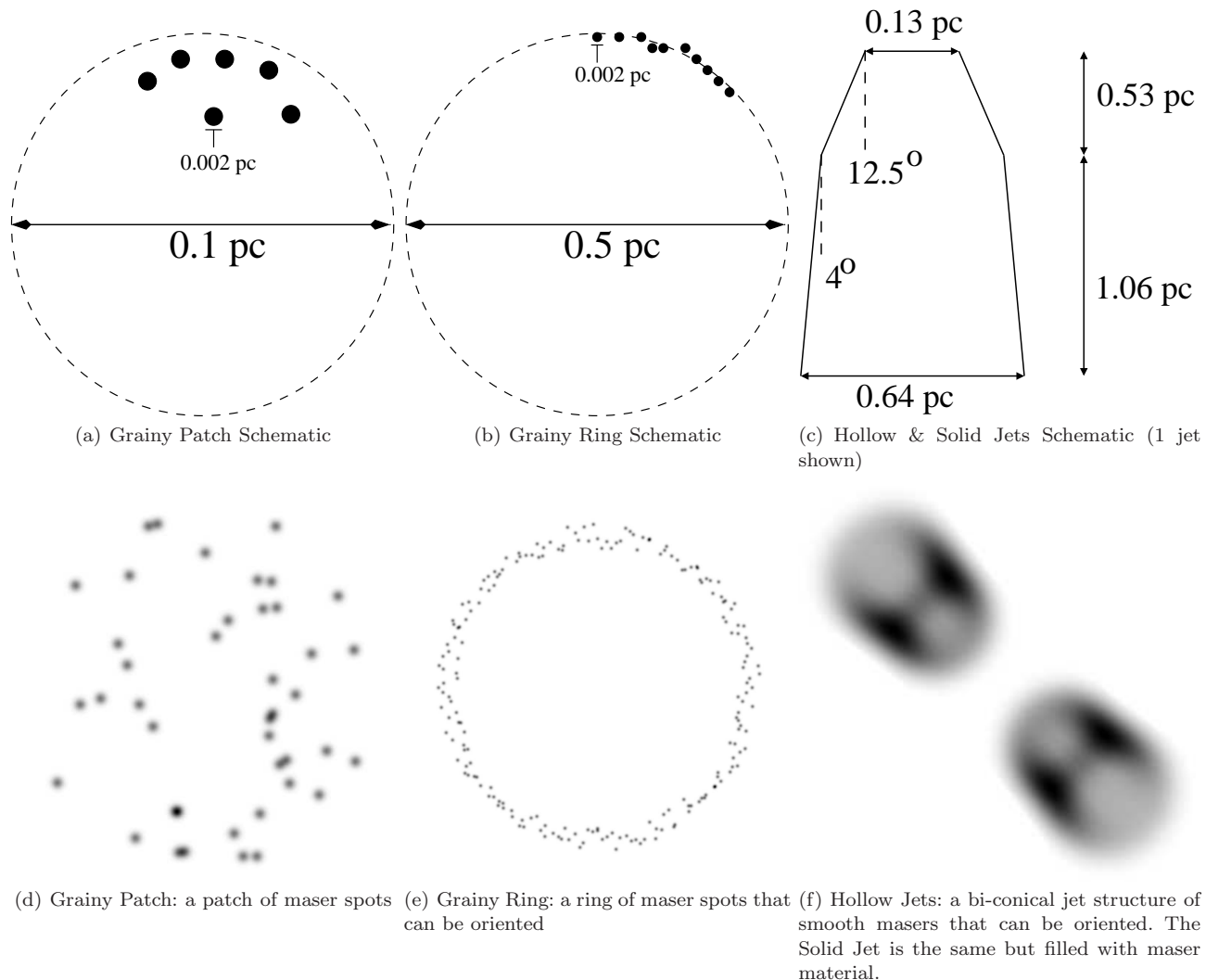


Figure 2. Schematics (a-c) and example images (d-f) of the three complex maser models (the Single Spot and Smooth Patch are not shown). Figures (a) and (d) show the Grainy Patch; (b) and (e) the Grainy Ring; (c) and (f) an example of the Hollow Jets, which is bi-conical as in (f), but since the jets are mirror images of each other only one schematic is shown in (c). The inclination of the jets in (f) is $i = 30^\circ$ South-East, relative to the magnification map as described in the text. The elements of the schematics are not to scale.

regions and darker areas are low magnification regions, and are relative to a mean magnification value. Notice that in the map there are thick lines or “trunks” of high magnification running up and down, these are the effects of the shear which imposes a directional trend on the map. It is not known what the true shear direction is for MG 0414+0534. The breakout box shows a region of the map at high resolution; one can see intricate patterns of light and dark which are called *caustics*. As a source moves across these the magnification varies, particularly when the source crosses a bright edge, leading to high magnification events. The Einstein Radius is defined in the next subsection.

Spatially extended sources are studied by convolving source models with the magnification map. To study the *differential microlensing* (Keeton et al. 2006) of frequencies emitted from separate regions of an extended source, each region is cut from the source and convolved separately to obtain a magnification for that frequency, and then combined to produce a microlensed spectrum. If this is done for

points along a path in the source plane then a time-varying spectrum for a source is obtained.

2.3 Microlensing distance and time scales

Microlensing systems are characterised by several time and spatial scales: the time between high magnification events, the duration of their occurrence, and the characteristic distance scale: the *Einstein Radius*. An Einstein Ring is generated from the simplest lensing situation, where a point source is directly behind a point lens, both perfectly in line with the observer. In that case the image that is produced is a circle around the lens. The observed angle θ_E between the lens and the circle circumference is given by

$$\theta_E = \sqrt{\frac{4GM}{c^2} \frac{D_{LS}}{D_L D_S}}, \quad (1)$$

where c the speed of light, G the gravitational constant, M the lens mass, D_{LS} , D_L and D_S the distance from lens

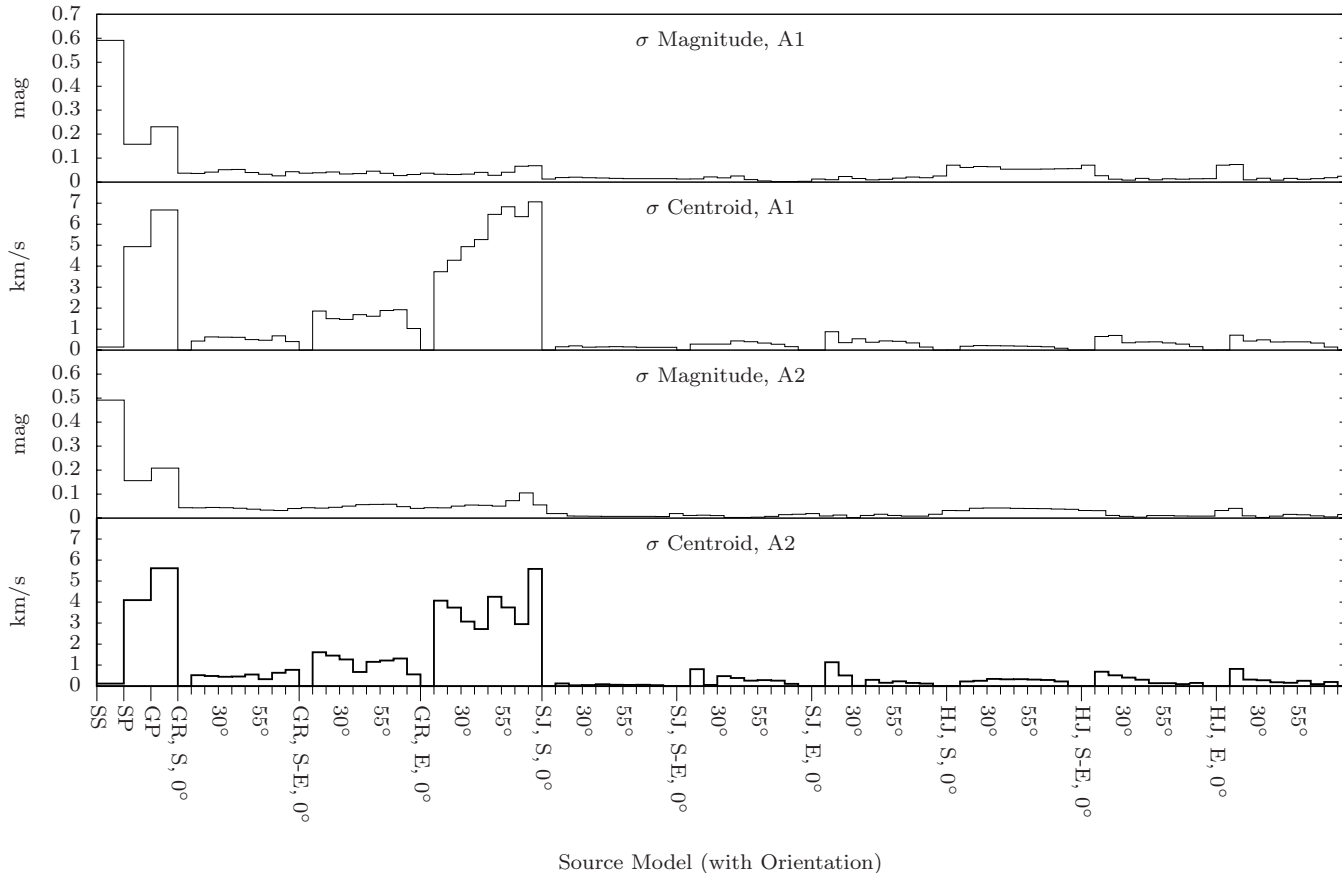


Figure 3. Measures of variability for the maser line in images A1 and A2, for all models, after microlensing. The top panel is the variation in the magnitude for image A1, the second panel is the variation in the spectrum velocity centroid for image A1. The next two panels are the same measures for image A2. In each panel is a plot of variability measure (vertical axis) as a function of source model, and orientation, for those that can be oriented (horizontal axis). Major tick marks indicate the model, inclination direction, and inclination angle e.g. GR=Grainy Ring, S=South, 0° is the angle. Models that cannot be oriented have no direction or angle. Following a major tick mark, minor tick marks indicate increasing inclinations for that model (not all angles shown). The same horizontal axis applies to all panels and is only listed on the bottom one. The vertical axis is indicated appropriately for each panel separately.

to source, observer to lens, and observer to source, respectively. Projecting θ_E onto the source plane produces a distance called the Einstein Radius (ER). Thus, the ER incorporates many aspects of the lens system, and is used as a length scale in microlensing analysis. It also indicates the size scale relevant for sources; sources of order 1 ER in size, and smaller, are more likely to be susceptible to microlensing than larger sources (see Refsdal & Stabell (1991, 1997) for the microlensing of large sources). For MG 0414+0534 we calculate the ER based on a point mass of $1 M_\odot$, since that size object will be used in our model galaxy. With a redshift for the lens of $z = 0.9584$ and for the quasar of $z = 2.639$, and assuming a concordance cosmology with $\Omega_0 = 0.3$, $\Lambda_0 = 0.7$ and $H_0 = 72 \text{ km s}^{-1} \text{ Mpc}^{-1}$, then $1 \text{ ER} \simeq 0.013 \text{ pc}$. The ER can be converted to a time scale if the relative velocity of the observer, lens, and source is known. Changes over time, rather than the ER, represent an observable of the lens system. (Chartas, Agol, Eracleous et al. 2002) derive a velocity of 170 km s^{-1} for converting source distance to time in MG0414+0534, so the time to travel 1 ER is 77 years.

3 METHOD

We use the inverse ray-shooting method (Kayser, Refsdal & Stabell 1986) developed by Wambsganss (1999) and parallelized by Garsden & Lewis (2010), to produce the magnification maps. Source models (detailed below) are convolved using Fourier transforms. All of these steps are executed using parallel processes and distributed memory on a supercomputer. Spectra are then extracted from a line across the map chosen to exhibit variability, and plotted for graphical examination. Parameters are extracted and reduced to measures of variability.

3.1 Magnification Maps

The convergence and shear for MG 0414+0534 are taken from Witt et al. (1995) and listed in Table 1. The maser has been observed in images A1 and A2, so only these will be modelled. For each image, two magnification maps are used with different resolutions, because the models represent masers of various sizes. The highest resolution maps span a source plane region of $2.5 \times 2.5 \text{ pc}^2$ ($185 \times 185 \text{ ER}^2$), the lower resolution maps cover $15 \times 15 \text{ pc}^2$ ($1115 \times 1115 \text{ ER}^2$). All

maps contain 20000×20000 pixels giving a source size resolution of $26 \times 26 \text{ AU}^2$ and $155 \times 155 \text{ AU}^2$ respectively, around the size of the solar system. All objects comprising the lens have masses of 1 solar mass (M_{\odot}). The number of objects is determined by the lens model and reaches 241,562,900 for the low resolution map for image A2. The map shown in Figure 1 is the $2.5 \times 2.5 \text{ pc}^2$ map for image A1, and the A2 map is similar in appearance. We assign directions to the map so that the orientation of maser models can be discussed. North (N) points up and East (E) is to the right, as in a land map. The directions are significant because they relate to the direction of shear that produces vertical patterns in the maps, which by our convention run N-S.

3.2 Maser source models

To model lensing of the maser in MG 0414+0534 we have chosen several types of source models of varying levels of complexity. We assume the maser material is transparent, and emitting isotropically. Because we wish to study the effect of microlensing on the spectrum and total flux, each model needs a size, a spatial flux emission profile, and a spatial frequency emission profile. The first two are described in Figure 2. The third is specified by the velocity profile of the source components, which translates to a frequency emission profile due to Doppler shifts. However, the maser velocities are not well-understood, as discussed in Section 2.1. Therefore we use the geometry of the model, and estimates based on observations, to obtain velocities for the masers, but scale them so that the line-of-sight velocity falls in a range of 100 km s^{-1} (except for the Single Spot which has no range). This is then sliced into 40 velocity intervals to produce a spectrum. All the model descriptions and results will refer to the velocities in the model, rather than frequencies. The next sections describe the different models.

3.2.1 Single Spot

This is the simplest model and is a single maser spot implemented as a 2-D Gaussian of total width 0.002 pc with a central velocity of -300 km s^{-1} and no velocity broadening. Since MG 0414+0534 is a powerful quasar we may assume that the spot size is at the high end of expected sizes for jet masers, so we chose the value of 0.002 pc , which also may approximate that of the spots in NGC 1052 (Claussen, Diamond, Braatz et al. 1998).

3.2.2 Two patches of masers

Some masers lie in a group on the side of a jet (e.g. NGC 1052: Claussen, Diamond, Braatz et al. 1998) with a fairly uniform velocity gradient from one side of the group to the other. Initially we approach this as an unresolved Smooth Patch, modelled as a 2-D Gaussian with a line-of-sight velocity gradient of -350 to -250 km s^{-1} from left to right. The total width of the patch is set at 0.1 pc , which is consistent with the size of other maser groups (e.g. Mrk348: Peck, Henkel, Ulvestad et al. 2003). As well as a smooth area, we use a group of spots, and replace the Smooth Patch with a collection of 49 spots called a Grainy Patch. The extent of the patch and the velocity profile remains the same,

but it consists of Single Spots, randomly located within a circular region. Figure 2 (a) has the schematic for the Grainy Patch, and (d) shows the resultant model, the Smooth Patch is not shown.

3.2.3 A Ring of Masers

If the jet in MG 0414+0534 is mostly face-on then it may be possible to observe masers situated in a ring around the jet. Figure 2 (b) shows the schematic of such a ring, where there are 200 Single Spots in a ring of diameter 0.5 pc . The location of each spot has been randomly perturbed from the true ring. The ring is assumed to lie $\sim 1.4 \text{ pc}$ along a conical jet, with an opening angle of 10° , allowing the ring to be oriented by orienting the jet. The jet has two degrees of freedom. Firstly, the angle of inclination determines whether the jet is perpendicular or parallel to the plane of the sky, in other words parallel to the plane of the magnification map. An inclination of $i = 0^\circ$ means the jet is pointing out of the map towards you, and $i = 90^\circ$ is fully side-on. Secondly, when the jet is inclined it may be pointing in a different compass direction on the map: South/East etc. The orientation of the ring has an impact on the lensing, as will be shown later. The ring at an inclination of 0° is shown in Figure 2 (e).

The jet material is outflowing, but the maser material in the ring is possibly turbulent and the velocity is not well known. However we will assume an overall bulk maser motion in a similar direction to the jet. Therefore we set the velocity of the masers to be in the same direction as the jet material they lie next to, but scaled so the line-of-sight velocity of the entire model falls between -350 and -250 km s^{-1} , the same as the for the patches. This range applies regardless of how the ring is oriented, except when it is face-on, in which case the line-of-sight velocity is the same around the ring and set to 300 km s^{-1} . We will call this model the Grainy Ring.

3.2.4 Continuous jet masers

This model consists of two identical jets in a bi-conical configuration outflowing from a quasar core. Each jet is 1.59 pc long, beginning at a base of width 0.13 pc with an opening angle of 25° for 0.53 pc , and then narrowing to 8° for 1.06 pc , producing a jet diameter of 0.64 pc at the limit of the model. The numbers are chosen because of the pixel resolution of the model. The schematic for one jet is shown in Figure 2 (c). The maser emission region begins 0.66 pc out along the jet axis and extends to the end. The maser material can exist all around the jet edge so it forms a truncated hollow cone, or it can be distributed through the jet, producing a solid cone. These will be called the ‘‘Hollow Jets’’ and ‘‘Solid Jets’’ models. If a cross section is cut through a jet perpendicular to its axis producing a ring or disk, the flux over that ring or disk remains constant as it travels out from the core with the jet material. The bi-conical jet structure can be inclined in the same way as the jet carrying the ring described in the previous subsection. Since both jets are conical outflows we use the same method for obtaining the maser velocities as for the Grainy Ring, but with some differences. Since the maser material extends along the jets

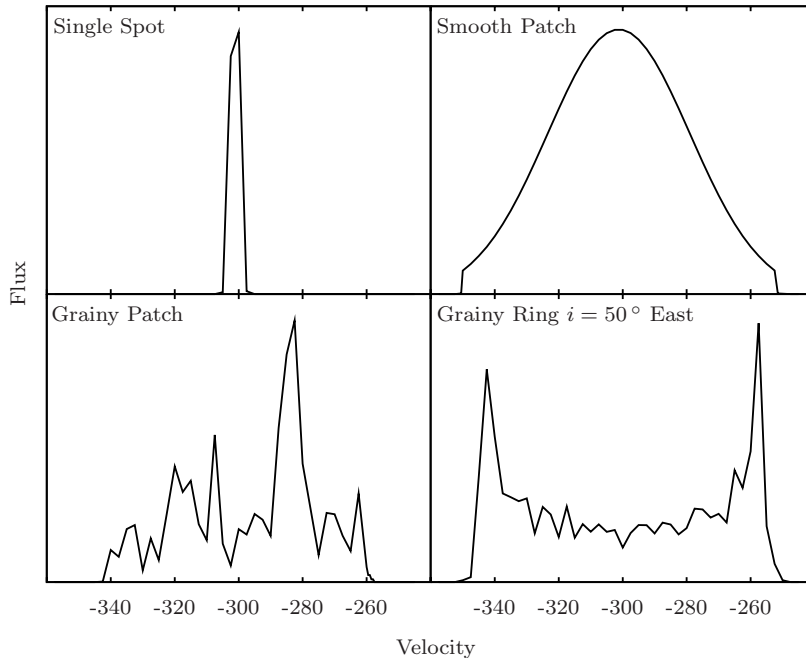


Figure 4. The spectra of the four simplest source models without lensing. The y-axis is the flux, the x-axis is the velocity present in the source model. Reading left to right, top to bottom, the spectra are for the models: Single Spot, Smooth Patch, Grainy Patch, Grainy Ring $i = 50^\circ$ East. The Single Spot has no velocity spread because we have not assigned it any, and produces a sharp peak (within the resolution of the slices). The Smooth Patch is a Gaussian and produces a Gaussian spectrum. The patch of spots, each one a Single Spot, produces a spectrum of many peaks reflecting the distribution of spots; at the right there is a region where there are a few more spots and which produces the highest peak. The ring produces a typical ring-generated spectrum with peaks at the lower and higher ends of the spectrum.

we set the velocity to be decreasing linearly with distance outwards, so the fastest material is near the core. Because the velocity range is centered around 0 km s^{-1} with a red- and blue-shifted jet on either side, the line-of-sight velocity will be scaled to a range of -50 to 50 km s^{-1} . An example of the Hollow Jets inclined to the South-East by $i = 30^\circ$ is shown in Figure 2 (f).

3.3 Spectrum and Source Path

We calculate the spectrum as the source travels across a region of high magnification on the map, specifically in a roughly S-E direction over one of the N-S “trunks” of high magnification caustics visible in Figure 1. This means the path will begin and end at areas of low magnification but pass across caustic regions of high density and complexity within the trunk. Such a path is a continuous and representative sampling of the microlensing effects that are represented by the map. The path is chosen by eye from examining the magnification maps at high resolution, and is slightly different for each magnification map used. This method produces a time-varying spectrum from which two parameters are extracted which are measures of variability:

- (i) A measure of the movement of the velocity centroid of the spectrum
- (ii) The variation in total magnitude

In both cases the standard deviation of the distribution of values is used as the variability measure.

4 RESULTS AND DISCUSSION

4.1 Time scale

The magnification map can be used to find the duration of, and the time between, high magnification events, which occur when the source passes over regions of high magnification in the map. Using a Single Spot for the source, we extract a light curve spanning the total width from East to West of the map for image A1. Scanning the light curve we find instances where the magnitude rises by 1, indicating the onset of an event. The shortest distance between two such instances is 0.034 pc , giving a time of 195 years between events. The shortest distance in which the magnitude rises by a value 1 is 0.003 pc , corresponding to a time of 17 years for the rise time of an event. This translates into significant variability for sources with small substructure like spots. For the spectrum of the Grainy Patch model, over a period of 17 years, statistical analysis shows that a typical variation of 0.12 mag and 2.0 km s^{-1} in velocity centroid is possible. These paths with variability in short intervals are more likely to be East-West across the North-South pattern of the shear visible in the map. A more detailed analysis is beyond this the scope of this paper but could be attempted in the future when more information is available, and using more sophisticated techniques (eg. Wyithe & Turner 2001).

4.2 Model Variability Statistics

The variability measures indicate how microlensing affects a source model as it moves behind the lens, i.e. along the

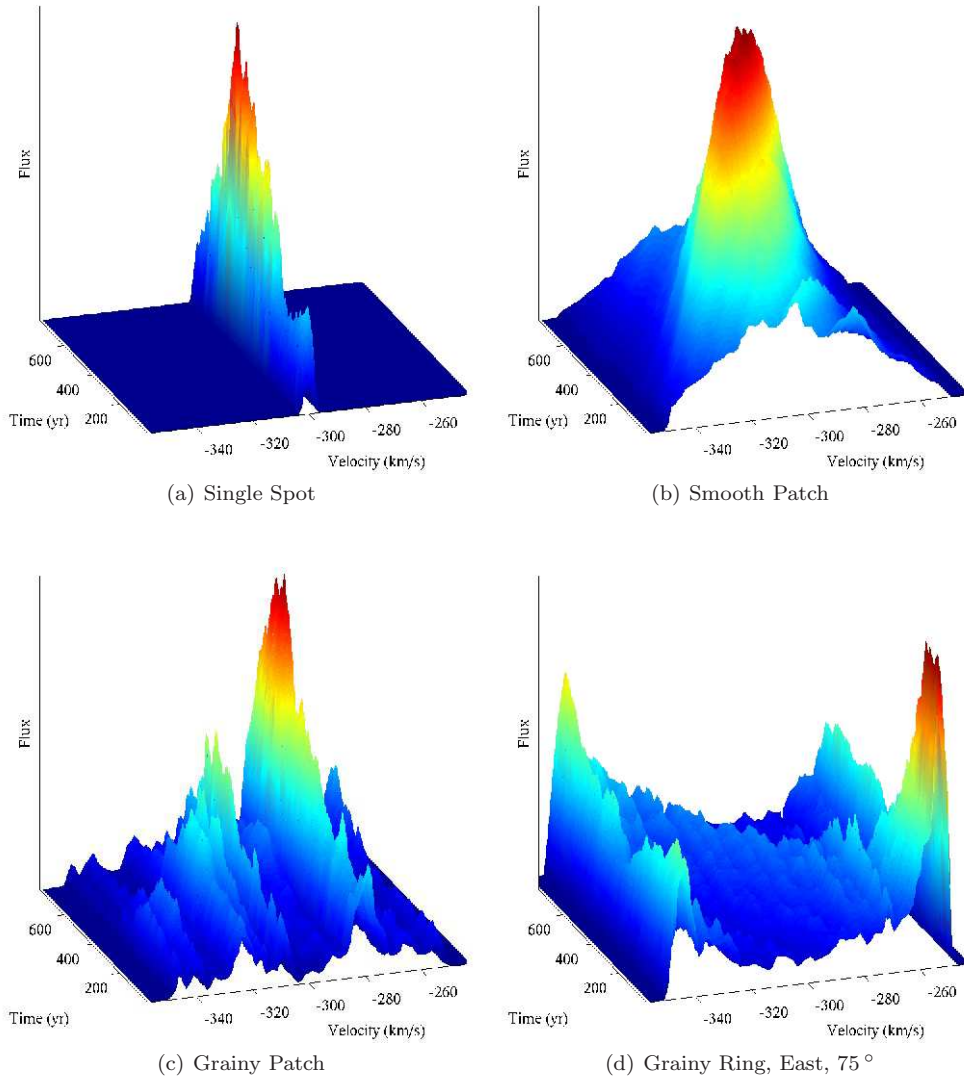


Figure 5. Spectra of the four simplest source models after lensing within image A1, corresponding in the same order to the spectra in Figure 4. As the source moves behind the lens a spectrum is captured at each point, these are concatenated to produce a continuous spectrum over time, so that the change can be seen. The Velocity axis is the velocity present in the source model. The Flux is the model flux. The Time axis indicates the passing of time as the source moves from an arbitrary zero point along a path we have chosen; a Time of 600 years corresponds to a source path distance of 0.1 pc (7.8 ER). For each model the spectrum doesn't not change radically; the overall shape is retained but small peaks may come and go. The Grainy Patch shows the most variability on statistical measures (Figure 3).

magnification map on the paths we have chosen. A summary of the results is depicted in the panels in Figure 3. Each panel is a graph of a variability measure (vertical axis) as a function of source model (horizontal axis). The top two panels show the light curve and velocity centroid variation for all models lensed within image A1, the next two are the same, but for image A2. The horizontal axis is the same for all panels, and only listed on the bottom panel. The vertical axis may be magnitude (mag) or velocity (kms^{-1}) for each panel, depending on the measure, and is labelled on the vertical axis of the panel. The horizontal axis values are codes indicating the model and orientation. Major tick marks are labelled with a code indicating the model: SS=Single Spot, SP=Smooth Patch, GR=Grainy

Ring, SJ=Solid Jet, HJ=Hollow Jet. For the models that can be oriented, this code is followed by a direction: S=South, S-E=South East, E=East, and then 0° , indicating the initial orientation of the model. The minor ticks that follow are increasing values of inclination, only 30° and 55° are shown. The Grainy Ring is inclined by 0° , 10° , 20° , 30° , 30° , 50° , 55° , 60° and 75° , the Jets by the same, as well as 90° . By scanning along the horizontal axis one can immediately see the relative variability of all the models, by the height of the graph in a panel.

From these graphs several general comments can be made. The Grainy Patch and Ring produce the highest variability in velocity centroid, both about the same value of 7 km s^{-1} , because they contain spots, i.e. small similar sub-

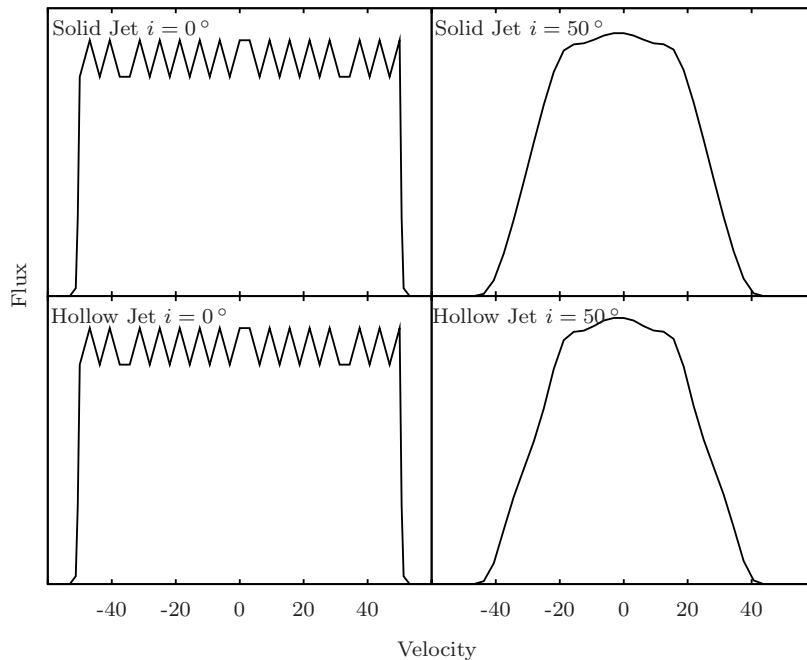


Figure 6. The spectra of the Solid Jets and Hollow Jets models without lensing. Reading left to right, top to bottom, the spectra are for the models: Solid Jet $i = 0^\circ$, Solid Jet $i = 50^\circ$ South-East, Hollow Jet $i = 0^\circ$, Hollow Jet $i = 50^\circ$ South-East. The Solid vs. Hollow models produce very similar spectra, because of the way the models are defined. Both of them change when the orientation is changed. A face-on ($i = 0^\circ$) inclination (left panels) produces a spectrum with an overall square-wave shape (to the resolution of the velocity slices), but when inclined (right panels) this transforms to a single peak, for both models. Only the inclination of $i=50^\circ$ South-East is shown here as a sample, the peaks get sharper with more inclination. One slight difference is that the Hollow Jet produces a sharper peak than the Solid Jets.

structure. However the Grainy Patch produces more magnitude variability relative to the Ring because it is smaller overall than the Ring. The Single Spot has no velocity centroid variation because its velocity range is below our resolution, but it has the highest magnitude variability (0.6), because it is the smallest-sized model. In contrast, the variability for the Jet models is low on both measures, because the models are large. The Smooth Patch has variability in both measures, less than the Grainy models and more than the Jet models, and an unexpectedly high variation in velocity centroid, considering it has no substructure. This variation will be explained in section 4.3.1 based on its spectral behaviour. Using a simple measure of variability per model – a sum of the rankings for centroid and magnitude for both images – the models in descending order of variability are: Grainy Patch, Grainy Ring (best at $i=75^\circ$ East), Single Spot, Smooth Patch, Hollow Jets, Solid Jets. The overall variability is similar for both images A1 and A2.

The orientation relative to the shear changes the variability for those models that can be oriented. Any orientation that produces structures parallel to the direction of shear in the map, i.e. N-S, will induce higher microlensing variability. This can be seen clearly in the centroid variability produced by the Grainy Ring in image A1 (Figure 3, top panel). As the direction changes from South to East, and with a high inclination, the ring presents a thin N-S profile, so the microlensing variability increases. In the case of the Jets, when they are N-S and highly inclined, the entire structure is in the direction of shear and so shows the most magnitude variability.

4.3 The forms of the spectra

The jets will be discussed separately from the other models since they have a different velocity spread and we will see they behave differently under inclinations.

4.3.1 Spot, Patches and Ring

The form of the spectra for these source models is given in Figure 4. The Single Spot shows a single peak with no velocity spread. The Smooth Patch produces a Gaussian spectrum, as it is a Gaussian model. The Grainy Patch has a multi-peaked spectrum due to the many small spots. The Grainy Ring shows the typical spectrum shape generated by a ring structure, with two peaks on the sides of the spectrum and a continuum between them, it is slightly broken because of the grainy nature. The spectra in Figure 4 are good representative examples as the spectra for all models retain those overall shapes even when inclined (remember the velocities have been normalised to always lie in the range of -350 to -250 km s^{-1}), and they also retain that overall shape when lensed. The changes that occur due to microlensing can be described either as an overall rise and fall or the introduction/disappearance/movement/magnification of small peaks or folds. Figure 5 contain typical examples of these phenomena, each spectrum is the lensed spectrum over time corresponding to the unlensed spectrum of Figure 4. The Single Spot shows how the magnification can rise and drop significantly when the quasar is travelling across a trunk of high magnification on the magnification map. The peak in the velocity axis rises from Time = 0 yrs to a maximum when

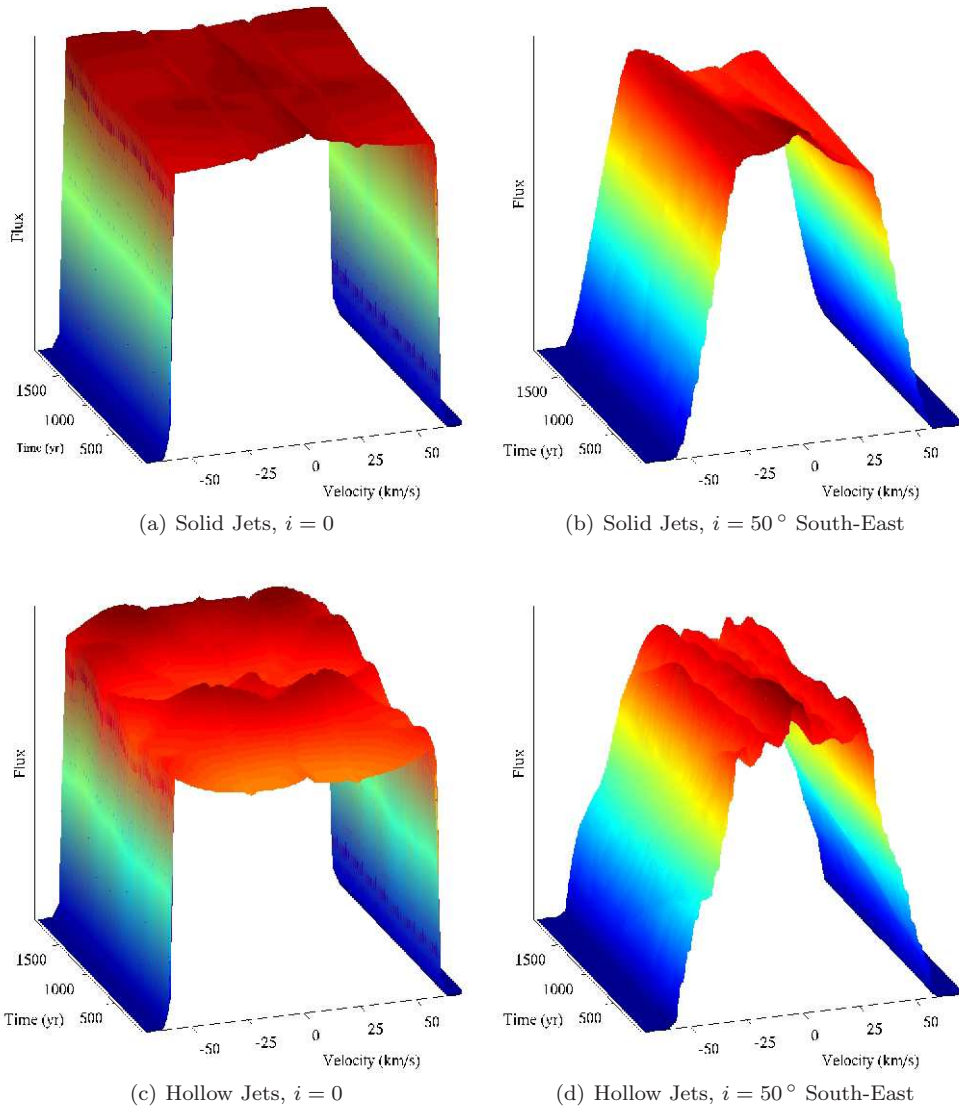


Figure 7. Spectra of the Jets source models, for image A1, after lensing. Each image corresponds to the spectrum in Figure 6. As the source moves behind the lens a spectrum is captured at each point, these are concatenated to produce a continuous spectrum over time, allowing the changes to be seen. The Velocity axis is the velocity present in the source model. The Flux is the model flux. The Time axis indicates the passing of time as the source moves from an arbitrary 0 point along a path we have chosen; a Time of 1500 years corresponds to a source path distance of 0.26 pc (19 ER). The models produce different spectra at different orientations but these are little affected by microlensing, and change little over time.

Time ~ 500 yrs, and then drops sharply after that. The Smooth Patch when lensed has a similar peak that rises and falls over time, but in the Velocity axis the peak is wide and smooth. One can also see that at Time=0 yrs, Velocity ~ -280 km s $^{-1}$ there is a fold, which diminishes over time. Also, although it is difficult to see in Figure 5(b), the entire peak for the Smooth Patch drifts from left to right on the Velocity axis, explaining the high centroid variability for this model; otherwise, it would have a very low centroid variability. The Grainy Patch has many peaks which rise and fall at different times, due to the substructure in the model, with an overall rise and fall as in the previous spectra. The Grainy Ring varies in flux but only shows some rise and fall at the edges, and at different times; it also shows an interior ridge formed by a peak that appears near Velocity ~ -260 km s $^{-1}$

at Time ~ 400 yrs and then moves to the other side of the spectrum arriving at Velocity ~ -340 km s $^{-1}$ at Time ~ 700 yrs, mimicking the drift in the Smooth Patch spectra. Other Ring orientations manifest similar behaviours. The rise and fall of the spectra, as in the Single Spot, will affect the total observed brightness of the maser line over time; the change of folds and peaks will affect the location of the velocity centroid of the broadened maser line over time. We do not see any dramatic changes in spectrum shape, based on viewing all the spectra obtained.

4.3.2 Jets

The jets are a bi-conical structure with identical outflowing jets on either side. The velocity profile is a linear veloc-

ity gradient out from the core, red- or blue-shifted on each side. With this model the form of the unlensed spectrum can change significantly depending on the orientation, but not over time, in contrast to the other models. Figure 6 shows two Solid Jets models and two Hollow Jets models before lensing. The Solid Jets and Hollow Jets when face-on produce an identical spectrum because the fluxes are normalized to be the same, and in this orientation the observed velocities will be the same. The apparent peaks are due to the resolution of the velocity slicing, if the resolution was very small the spectra would be smooth and flat. When the same models are inclined by 50° , they both transform into a single peak, which becomes sharper the more inclined they are. Figure 7 shows the same models after lensing, and it is clear there is little change due to lensing, because the jet structure is large compared to the Einstein Radius and does not undergo significant microlensing. There is some variation right at the peak with small folds coming or going, but the flux is fairly constant, indicating little variation in the spectrum over time. What is of more interest with this structure is the spectra produced by different inclinations. Starting with a square wave when face-on, *both* the Solid and Hollow Jets spectra can merge towards a single smooth peak whether lensed or unlensed, with microlensing producing slight variations at the peak over time. This has implications for matching source models with the observed spectra.

4.4 Comparison with observations

Several factors make it difficult to choose which of our models can produce the observed maser line. Firstly, in a source with multiple components, some components may be de-magnified by microlensing and thus not appear in the spectrum; observation over long time scales may reveal these. Secondly, the entire maser spectrum may not be clearly visible because of noise in the signal or components of the maser spectrum may lie below the detection limit. Thirdly, the observed line is coincident with an HI absorption trough (Barvainis et al. 1998; Curran et al. 2007), possibly masking a different spectral signature. Fourthly, the observed line is the combined spectra of both image A1 and A2. Although the images have similar microlensing properties and similar variability measures, the spatial correlation between the high resolution maps for A1 and A2 is only 56%. This indicates that some high magnification events do not correlate between the two images in either magnification or epoch of observation. It would be preferable to observe the maser line in A1 and A2 separately, since this will provide extra information to use to distinguish between models. Naturally the last three issues are due to the technical limitations of the observation, and will improve in the future.

To match the observation, we look for models that have produced a single peak. The Single Spot has a peak, but it is not likely to be realistic since masers in jets usually occur in groups of spots. The Smooth Patch produces a smooth peak that is broad and maintains its shape, rising and falling with changing magnification, although it may drift around in velocity. Therefore if observation shows little change in shape, but changes in flux and centroid, the Smooth Patch is indicated. The Grainy Patch produces several peaks depending on the arrangement of maser spots, and our model deliberately includes a large peak which could match the observa-

tion. The existence of other smaller peaks in the model spectrum, but not seen in the observed spectrum, does not lessen the likelihood for the Grainy Patch. Such peaks may be currently de-magnified or lie below the noise, either within the current observed line or at lower or higher velocities outside it. In the latter case the Grainy Patch model remains valid as our velocity range is artificial and can also be expanded. If future observations resolve smaller peaks, or peaks appear over time, the Grainy Patch model is consistent with the observation. The Grainy Ring produces two clear peaks at the higher and lower ends of the spectrum and we do not observe enough microlensing variation that could produce a single peak, so this model appears less likely. Interestingly, the Jet models are capable of producing a smooth single peak, which varies insignificantly over time in either velocity or flux. If the observed maser spectrum exhibited the same properties, then the Jet models would be consistent with the observation. However, an inclination of more than 50° is required to produce such a spectrum, and since the quasar is believed to be not so inclined, this mitigates against the Jet models.

4.5 Magnifications

A search for masers in other lensed AGNs has not been successful (McKean et al. 2010), partly due to the lack of required sensitivity in existing telescopes, but that will improve. However, predictions have been made about the detectability of lensed AGN masers assuming a magnification of 35 for MG 0414+0534 based on analytic strong lensing models (Impellizzeri, McKean, Castangia et al. 2008; Trotter, Winn & Hewitt 2000). Using the Single Spot as a source, we found a peak magnification of 91 can be achieved in image A2, with a magnification of 35 or better achieved 22% of the time. If long-term observing, combined with models of the system, show that the typical magnification is lower than 35, this indicates the maser is more intrinsically luminous than previously thought, with consequences for the rate of detection.

5 CONCLUSIONS

Observations of jet masers in active galaxies indicate that the masers typically exist in a group with a velocity range of the order 100 km s^{-1} . The maser in MG 0414+0534 consists of a single peak. This is not consistent with a group of maser spots that produces multiple peaks, unless some peaks are lost in noise, or currently de-magnified, which is certainly possible. On the other hand the observation could be a smooth patch of masers, or a smooth distribution through the inner parts of the quasar jets, all of which also produce a single peak. A patch of spots will produce the most variability, in both velocity centroid and magnitude, the smooth patch will produce less – it may drift in velocity but remain fairly constant in shape – the jets will not change at all. A source with substructure like a patch of spots could produce changes in the spectrum within a couple of hundred years, lasting for 10-20 years. These results are just the beginning of the numerical analysis of this lensed maser, and continuing work would include:

- Developing physically consistent models based on future observations and new understanding of masers
- Developing statistical tools for the extraction of histograms, structure functions, and other data from the high resolution magnification maps

but it would be prudent to wait for observations that have a higher sensitivity and resolution of flux and velocity, and in particular that are able to detect the maser in images B and C. A long-term monitoring program should be carried out on this source, either with a large single dish or a sensitive VLBI array (e.g. the European VLBI Network) with higher resolution than the original Effelsberg observations, with the following aims:

- monitoring should be conducted on monthly time scales to pick up short term fluctuations as well as building statistics for long term variability
- the A1 and A2 image spectra should be separated, which allow a comparison of the spectral behaviour between the two images for all the models, adding information that may constrain the choice of model
- observations at higher spectral resolution may allow a more accurate determination of the spectral shape; differential fluctuations over time due to substructure will help to determine the morphology of a maser group.

ACKNOWLEDGMENTS

Computing facilities were provided by the High Performance Computing Facility at The University of Sydney. This work is undertaken as part of the Commonwealth Cosmology Initiative (www.thecci.org), and funded by the Australian Research Council Discovery Project DP0665574. We thank the anonymous referee whose comments improved the quality of this paper.

REFERENCES

- Bate N. F., Webster N. F., Wyithe J. S. B., 2008, *MNRAS*, 381, 1591
- Bate N. F., Floyd D. J. E., Webster R. L., Wyithe J. S. B., 2008, *MNRAS*, 391, 1955
- Barvainis R., Alloin D., Guillobeau S., Antonucci R., 1998, *ApJ*, 492, L13
- Biretta J. A., 1993, in Burgarella D., Livio M., O’Dea C. P., eds, *Proc. STScI Symp. 6, Astrophysical Jets*. Cambridge University Press, Cambridge, p. 263
- Chang K., Refsdal S., 1979, *Nature*, 282, 561
- Chartas G., Agol E., Eracleous M., Garmire G., Bautz M. W., Morgan N. D., 2002, *ApJ*, 568, 509
- Claussen M. J., Diamond P. J., Braatz J. A. et al., 1998, *ApJ*, 500, L129
- Curran S. J., Darling J., Bolatto A. D., Whiting M. T., Bignell C., Webb J. K., 2007, *MNRAS*, 382, L11
- Eigenbrod A., Courbin F., Meylan G., Agol E., Anguita T., Schmidt R. W., Wambsganss J., 2008, *A&A*, 490, 933
- Garsden H., Lewis G. F., 2010, *NewA*, 15, 181
- Gaudi, B. S., Bennett, D. P., Udalski, A., 2008, *Science*, 319, 927
- Huchra J., Gorenstein M., Kent S., Shapiro I., Smith G., Horne E., Perley R., 1985, *AJ*, 90, 691
- Impellizzeri C. M. V., McKean J. P., Castangia P. et al., 2008, *Nature*, 456, 927
- Inada N., et al., 2005, *AJ*, 130, 1967
- Kayo, I., Inada, N., Oguri, M., et al., 2010, *AJ*, 139, 1614
- Kayser R., Refsdal S., Stabell R., 1986, *A&A*, 166, 36
- Keeton C. R., Burles S., Schechter P. L., Wambsganss J., 2006, *ApJ*, 639, 1
- Kochanek C. S., Dai X., Morgan C. et al., 2009, in Babu G. J., Feigelson E. D., eds, *Proc. ASP Conf. 371, Statistical Challenges in Modern Astronomy IV*. ASP, San Francisco, p. 43
- Kovalev Y. Y., Lister M. L., Homan D. C., Kellermann K. I., 2007, *ApJ*, 668, L27
- Lawrence C. R., Elston R., Januzzi B. T., Turner E. L., 1995, *AJ*, 110, 2570
- Lewis, G. F., Irwin, M. J., Hewett, P. C., & Foltz, C. B. 1998, *MNRAS*, 295, 573
- Lewis G. F., Gil-Merino R., 2006, *ApJ*, 645, 835
- McKean J. P., Impellizzeri C. M. V., Roy A. L., Castangia P., Samuel F., Brunthaler A., Henkel C., Wucknitz O., 2010, *arXiv*, arXiv:1009.0290
- Miroshnichenko A. P., 2005, *A&AT*, 24, 409
- Moran J. M., Humphreys E., Greenhill L. et al., 2007, in Chapman J., Baan W., eds, *Proc. IAU Symp. 242, Astrophysical masers and their environments*. Cambridge University Press, Cambridge, p. 391
- Mortonson M. J., Schechter P. L., Wambsganss J., 2005, *ApJ*, 628, 594
- Myers S. T., et al., 1999, *AJ*, 117, 2565
- Paczynski B., 1986, *ApJ*, 301, 503
- Peck A. B., Henkel C., Ulvestad J. S. et al., 2003, *ApJ*, 590, 149
- Refsdal, S., & Stabell, R. 1991, *A&A*, 250, 62
- Refsdal, S., & Stabell, R. 1997, *A&A*, 325, 877
- Ros E., Kadler M., 2008, *JPhCS*, 131, 012056
- Sand, D. J., Treu T., Ellis, R. S., Smith, G. P., Kneib, J-P, 2008, *ApJ*, 674, 711
- Schechter P., Wambsganss J., 2002, *ApJ*, 580, 685
- Schechter P., Wambsganss J., Lewis G. F., *ApJ*, 2004, 613, 77
- Schneider P, Ehlers J, Falco EE. *Gravitational Lenses*. Springer-Verlag: Berlin 1992.
- Shalyapin V. N., 2001, *AstL*, 27, 150
- Trotter C. S., Winn J. N., Hewitt J. N., 2000, *ApJ*, 535, 671
- Turner E. L., et al., 1989, *BAAS*, 21, 718
- Walsh D., Carswell R. F., Weymann R. J., 1979, *Nature*, 279, 381
- Wang C-C., Zhou H-Y., 2009, *MNRAS*, 395, 301
- Wambsganss J., 1990, Ph.D. Thesis, Ludwig Maximilian University, Munich.
- Wambsganss J., 1998, *LRR*, 1, 12
- Wambsganss J., 1999, *J Comput Appl Math*, 109, 353
- Wambsganss J., 2006, in Meylan, G., Jetzer, P., North, P., eds, *Gravitational Lensing: Strong, Weak and Micro: Saas-Fee Advanced Course 33*, Springer, Berlin, p 453
- Wambsganss J., 2006, *AnP*, 518, 43
- Wambsganss J., 2010, in Klioner S. A., Seidelmann P. K., Soffel M. H., eds, *Proc. IAU Symp. 261, Relativity in Fundamental Astronomy: Dynamics, Reference Frames, and*

- Data Analysis. Cambridge University Press, Cambridge,
p. 249
- Wambsganss J., Paczynski B., 1991, *AJ*, 102, 864
- Wambsganss J., Paczynski B., Schneider P., 1990, *ApJ*,
358, L33
- Willis J. P., Hewett P. C., Warren S. J., Dye S., Maddox
N., 2006, *MNRAS*, 369, 1521
- Witt H. J., Mao S., Schechter P., 1995, *ApJ*, 443, 18
- Wyithe J. S. B., Turner E. L., 2001, *MNRAS*, 320, 21
- Young P., 1981, *ApJ*, 244, 756
- Zwicky F., 1937, *Phys. Rev.*, 51, 290

This paper has been typeset from a $\text{T}_{\text{E}}\text{X}/\text{L}^{\text{A}}\text{T}_{\text{E}}\text{X}$ file prepared
by the author.